ROYAL SOCIETY
OF CHEMISTRY

# PAPER

Check for updates

# A silver metal–organic cage with antibacterial activity for wound healing†

Linlin Chen,[a] Jing Cheng,[a] Longjie Wang,[b] Wenwen Fan,[b] Zhixiang Lu*[c] and Liyan Zheng [ID] *[b]

Bacterial infection is one of the most threatening diseases in humans and can result in tissue necrosis, inflammation, and so on. Although a large number of antibacterial materials have been developed, there are still some disadvantages in this field, including decreasing antibacterial activity in the aqueous solution or a short duration of time. Herein, a metal–organic cage named Ag-TBI-TPE with excellent antibacterial activity was prepared and applied in wound healing. Owing to the photosensitive production of the toxic ROS species and the positive charge of the surface, the Ag-TBI-TPE cage exhibits high antibacterial activity, especially under UV irradiation. It could accelerate the healing process of the infected wounds *in vivo* with satisfactory biocompatibility and bio-safety. The results indicated that after treatment with the Ag-TBI-TPE cage, with and without UV irradiation, the healing rates of wounds infected by *E. coli* and *S. aureus* were 89.59% and 93.05%, and 83.48% and 90.84%, respectively, which were much higher than those shown by the positive control group at 51.38% and 67.74%, respectively. This study not only sheds light on a design idea for a new antibacterial material but also further expands the potential application field of metal–organic cages.

## Introduction

Bacterial infections pose a great threat to human health and environmental safety,[1–5] for example, severe diarrhea and food poisoning are caused by *E. coli* and *S. aureus*, respectively.[6,7] However, the rapid increase of new bacterial strains and bacterial antibiotic resistance brings a big challenge and cost burden on medical treatments.[8] In order to further solve bacteria-induced diseases, it is urgently required to develop highly efficient and broad-spectrum antibacterial drugs.[9–12] To date, many antibacterial materials have been obtained as an alternative to antibiotics, including metal ions, photo-sensitizers, antimicrobial peptides, and hydrogels. The antibacterial mechanism of these materials could be linked to the inhibition of the cell wall synthesis, interaction with the cell membrane, interference of protein synthesis or inhibition of nucleic acid transcription and replication, *etc.*[13–17]

In photodynamic therapy (PDT), the photo-sensitizer can absorb light to produce singlet oxygen ($S_1$) and further transform to triplet excited states ($T_1$), which leads to the production of toxic reactive oxygen species (ROS) to effectively kill bacteria.[18–20] However, most of the reported photo-sensitizers tend to aggregate with bacteria in water, which will cause fluorescence quenching and decrease ROS production, thereby affecting their image quality and treatment effects.[19,21–23] Some AIE molecules have shown potential application in imaging PDT due to their increasing ROS production property upon aggregation.[24–28] For example, the Tang group synthesized a new antibacterial material TriPE-NT that was composed of AIE unit TriPE and an antibacterial unit, NT, which showed a significantly improved antibacterial activity. Combining the antibacterial activity of NT and the ROS generation ability of TriPE and TriPE-NT could not only maintain the excellent antibacterial property of NT but also increase the antibacterial activity under light irradiation.[24] These studies have provided a new strategy to design multifunctional antibacterial materials to broaden the application field.

Metal–organic cages possess the advantages of good photophysical stability, facile modulation, and the ability to introduce a variety of functional groups, which introduce rich properties and broaden their applications in many fields.[29–31] Introducing AIE units to the metal–organic cage could make it exhibit good optical properties in both dissolved and aggregate states by inhibiting its molecular rotation.[32] Designing new metal–organic cages with AIE units as photosensitizers in PDT therapy has a great application potential;[33–37] however, the research on this topic is still rare.

In previous studies, our group reported a metal–organic cage (Ag-TBI-TPE cage) formed with the AIE ligand (TPE-TBI) and silver cation, which exhibited satisfactory optical properties in

*[a] QuanZhou Medical College, Quanzhou, Fujian 362000, China*

*[b] School of Chemical Science and Technology, Key Laboratory of Medicinal Chemistry for Natural Resource, Yunnan University, Kunming 650091, China*

*[c] School of Pharmaceutical Sciences, Xiamen University, Xiamen 361102, China*

both dissolved and aggregate states in the aqueous solution.[38] Because it possessed fine optical behavior, high stability, and positive charge, it could be used as an antibacterial material because bacterial membranes are generally negatively charged. Actually, the Ag-TBI-TPE cage displayed a significant antibacterial property, and this activity could be further increased under light irradiation conditions towards *E. coli* and *S. aureus*. Moreover, the Ag-TBI-TPE cage simultaneously showed excellent biological safety and compatibility, which favors its application *in vitro* and *in vivo*.

# Experimental

## Reagents

Silver nitrate and dimethyl sulfoxide-$d_6$ were purchased from Sigma Aldrich. *N,N*-dimethylformamide (DMF), 1,4-dioxane, tetrahydrofuran (THF), 2,2′-azinobis-(3-ethylbenzothiazoline-6-sulphonate) (ABTS), acetone, and ethyl acetate (EtOAc) were purchased from Energy Chemical company and used without further purification. Luria-Bertani (LB) was purchased from Tansoole. *Escherichia coli* (ATCC 25922) and *Staphylococcus aureus* (ATCC 25923) were obtained from Guangdong Huankai Microbiology Technology Co., Ltd Double-distilled water was purified using the Milli-Q system and used throughout the experiments.

## Characterization of MOC

Scanning electron microscopy imaging (SEM) was performed using a QUANTA200 scanning electron microscope (FEI, USA) operated at 30 kV. Optical density (OD) values were measured using a microplate reader (M200 PRO NanoQuant). The zeta potential was measured on a NanoBrook 90 plus Zeta (Brookhaven, American) instrument. UV-vis absorption spectra were recorded on a UV-240IPC UV-vis spectrometer (Shimadzu, Japan).

## Synthesis of the Ag-TBI-TPE cage

The Ag-TBI-TPE cage was synthesized according to our previous report.[38,39] In brief, TBI-TPE ((1,1,2,2-tetrakis(4-(1*H*-benzo[*d*]imidazol-2-yl)phenyl)ethane, 20 mg, 0.025 mmol) was dissolved in 20 mL of methanol solution, and silver nitrate (17 mg, 0.1 mmol) was dissolved in 100 μL water; then, the silver nitrate solution was then added dropwise to the TBI-TPE solution under continuous stirring at room temperature. Immediately, a bright yellow solid was formed and after 5 minutes, the solid was centrifuged at 14 000 rpm for 1 minute, washed with methanol and diethyl ether separately. The resulting powder was dried at room temperature and named the Ag-TBI-TPE cage.

## Antibacterial activity test

Filter papers (6 mm diameter) were immersed in 0.1 mM Ag$^+$, TBI-TPE, and Ag-TBI-TPE cage for 30 min, respectively. 100 μL bacterial suspensions ($2 \times 10^8$ CFU mL$^{-1}$, colony forming units) of *E. coli* and *S. aureus* were spread onto nutrient agar plates using a sterile pipette, and the filter papers were then placed on the agar surface. The plates were incubated at 37 °C overnight and the diameters of the inhibition zones were measured. Each experiment was carried out three times in parallel.[40]

The bacterial suspensions of *E. coli* and *S. aureus* ($2 \times 10^8$ CFU mL$^{-1}$) interacted with different concentrations of Ag$^+$ and Ag-TBI-TPE cage (0.5–10 μM) for 10 min, 20 min, and 30 min. 100 μL of the above bacterial suspensions were taken out and 900 μL of sterilized water was added. The diluted bacterial suspensions were cultured on the nutrient plates at 37 °C for 24 h and the numbers of colonies were counted. Furthermore, the antibacterial rate under UV irradiation (370 nm) was measured using the same method. The antibacterial ratio (%) = (number of CFUs in the control group − number of CFUs in the experimental group)/(number of CFUs in the control group) × 100%. Each experiment was repeated three times in parallel.

## Optical density test

Firstly, the bacterial colony was activated in LB nutrition solution and cultured at 37 °C for 18 h. Then, 100 μL of the activated suspension was removed and 5 mL LB was added. Next, 180 μL of the above bacterial solution was mixed with the same volume of Ag$^+$, Ag-TBI-TPE cage, and sterilized water, respectively, and added in the 96-well plates and the optical density values were measured at 600 and 260 nm.[41] For the concentration of materials, each experiment was repeated three times in parallel.

## Acute toxicity test

Thirty Kunming mice (the experiment center of Quanzhou Medical College, Fujian, China), weighing between 20 g and 25 g were randomly divided into 3 groups. To evaluate the acute toxicity of materials, $1 \times 10^5$ mg kg$^{-1}$ (5 μM) of the Ag-TBI-TPE cage, sterilized physiological saline, $2.375 \times 10^{-3}$ g mL$^{-1}$ DMF, were used as the experimental group, negative group, and control to carry out the experiments, respectively. 10 mice in a group were injected with 400 μL of the sample solution, sterilized physiological saline, and DMF in enterocoelia. Then, their breathing, movement, defecation, eating, death, and so on were observed and recorded for 7 days; in the meantime, the weight of the mouse was also recorded (Table 1).

## Hemolysis assay

RBCs from the blood (5 mL) of a healthy rabbit were obtained by centrifuging the sample at 1000 rpm for 10 min and washed

**Table 1** Observation index of the animal reaction in acute toxicity test

| Degree | Reaction |
| --- | --- |
| None | No toxic reaction |
| Subtle | Mild symptoms, but no reduction in exercise, difficulty breathing or abdominal stimulation |
| Medium | Abdominal stimulation, dyspnea, reduced exercise, drooping eyelids, diarrhoea (weight reduced to 15–17 g) |
| Severe | Exhaustion, cyanosis, and tremors, severe abdominal irritation, ptosis of the eyelids, breathing difficulties (sudden weight loss, generally below 15 g) |
| Death | Dead |

with saline (0.9% NaCl) three times, then resuspended using normal saline (100 mL) to prepare 2% erythrocyte solution. Then, mixtures of 0.5 mL of different concentrations of Ag-TBI-TPE cages and 0.5 mL 2% erythrocyte solutions were incubated at 37 °C for 3 h. The supernatants were then obtained by centrifugation at 1000 rpm for 10 min, transferred to a 96-well plate, and the absorbance at 540 nm was measured. RBCs in normal saline and distilled water were used as negative and positive controls, respectively.

Hemolysis (%) = (mean of the absorbance value of the treated group − mean of the absorbance value of the negative control group)/(mean of the absorbance value of the positive control – mean absorbance value of the negative control group) × 100%. Each experiment was carried out three times in parallel.

### MTT bioassay

The cytotoxicity of the Ag-TBI-TPE cage was evaluated using a direct contact method according to the ISO10993-5 standard test using L929 cells. Preparation of 96-well plates for cell culture: L929 cells were counted using the Trypan blue exclusion method and quantified using an automated cell counter. The cells were plated in 96 well-flat bottom plates using a multichannel pipette. Each 96-well plate was partitioned into columns in the following way: (1) cells incubated in the culture medium alone were set as a control; (2) test cells were incubated in the culture media with Ag-TBI-TPE cage samples at different concentrations ($5 \times 10^{-6}$, $1 \times 10^{-5}$, and $5 \times 10^{-5}$ mol L$^{-1}$). All conditions were tested in triplicate wells, and each experiment was repeated three times. Cells were prepared as single-cell suspensions for testing. Cells were plated in each of 96 wells ($1.0 \times 10^5$ cells per mL) and incubated in the DMEM medium ($1.0 \times 10^5$ cells per mL) under standard culture conditions for 24 hours. Thereafter, the cells were incubated for up to 72 h after, which the cell viability was measured using the MTT (5 mg mL$^{-1}$) assay. The results were expressed in terms of cell viability (24 h, 48 h, and 72 h, respectively). The absorption of the samples was measured at 490 nm. Cell viability (IC$_{50}$) was determined by the concentrations of analytes of the target, resulting in 50% inhibition of cell growth. All experiments were performed in triplicate.

### Wound healing *in vivo*

Animal experiments were reviewed and approved by the Animal Investigation Ethics Committee of the Quanzhou Medical College. Sprague-Dawley (SD) male rats (180–250 g) were obtained from Shanghai SLRC Laboratory Animal Co. Ltd, China, to evaluate the effect of the Ag-TBI-TPE cage on infected wound healing of the skin. 20 healthy male SD rats were anesthetized and shaved and then randomly divided into four groups. Two full-thickness round wounds (1 cm × 1 cm) were created on the back of each rat.[41,42] For group I, the wounds were treated with the physiological saline as a negative control. The group II was infected without treating it as a positive control. 200 μL *S. aureus* suspension ($1 \times 10^8$ CFU mL$^{-1}$) was slowly added to the left wound and 200 μL *E. coli* suspension ($1 \times 10^8$ CFU mL$^{-1}$) was

slowly added to the right wound. For group III, the wounds were infected with *S. aureus* and *E. coli* and the infection operation was the same as group II. After 12 h, the infection wounds were treated with Ag-TBI-TPE cage ($5 \times 10^{-6}$ mol L$^{-1}$, 100 μL). For group IV, the wounds were infected with *S. aureus* and *E. coli* and the infection operation was the same as in group II. After 12 h, the infection wounds were treated with Ag-TBI-TPE cage ($5 \times 10^{-6}$ mol L$^{-1}$, 100 μL) and irradiated for 30 min using UV at the same time. After the treatment, samples were taken from the wounds of the four groups for culture and observation. The physiological saline and Ag-TBI-TPE cages were changed every day. The wound size was measured and recorded with a digital camera every day until the seventh day. Changes in the wound area in each group were analyzed using Image-Pro Plus.

The wound healing rate = (mean of initial wound area − mean of current wound area)/mean of current wound area × 100%.

### Histologic analysis

The wound tissues, post-operation, were collected from each group of rats on day 3 and day 7. The major organs including the heart, liver, spleen, lung, and kidney were excised from each group of rats on day 7. All these samples were fixed with 10% formalin to prepare the slides. After staining with hematoxylin and Eosin (H&E), the histological images were acquired on an optical microscope (Nikon Eclipse T1-SR).

## Results and discussion

### Synthesis and characterization of the Ag-TBI-TPE cage

The synthesis procedure of the Ag-TBI-TPE cage was referred to in our previous reports, and the obtained positively charged Ag-TBI-TPE cages were easy to disperse in water.[38] PXRD and FTIR were first measured to confirm the structure of the Ag-TBI-TPE cage. The Ag-TBI-TPE cages showed sharp PXRD patterns, which were in accordance with the simulated patterns from single crystal data, illustrating their successful synthesis. In addition, it can be observed that the characteristic peak of $\nu_{C=N}$ at 1640 cm$^{-1}$ became wider, which indicated that the Ag-TBI-TPE cage was successfully prepared due to the coordination of Ag with N atoms in the benzimidazole group. Moreover, there was a new peak at 1390 cm$^{-1}$, which confirmed that the Ag-TBI-TPE cage contained nitro groups (Fig. S1†). To further verify the result, XPS measurements were performed; it was obvious that after interacting with silver cations, a new peak belonging to Ag 3d appeared, which was ascribed to the coordination effect. Then, binding energy peaks were observed at 368.8 and 374.7 eV for Ag 3d$_{5/2}$ and Ag 3d$_{3/2}$, respectively, which are the typical values for Ag(ɪ). Furthermore, N 1s can be divided into –C=N (398.0 eV) and –C–N (401.5 eV) in TBI-TPE; while there were four states of N 1s in Ag-TBI-TPE. The binding peaks were 399.0, 399.5, 400.5, and 406.5 eV, ascribed to the Ag–N coordinate bond, –C=N, –C–N, and nitrate, respectively (Fig. S2†). These results demonstrated that the Ag-TBI-TPE cage was obtained through the coordination effects of silver ions with nitrogen atoms in the organic ligand.

It has been reported that as the photo-sensitizer, aggregated state AIE molecules could increase ROS production due to the inhibition of nonradiative transition.[25,43] Inspired by this report, we assumed that the Ag-TBI-TPE cage was a typical metal coordination compound with ICT and AIE characteristics, which could promote the production of ROS. To confirm this, a characteristic color reaction catalyzed by the Ag-TBI-TPE cage was performed. As shown in Fig. 1, after mixing ABTS with Ag$^+$, TBI-TPE, and Ag-TBI-TPE cage, only the Ag-TBI-TPE cage group with light irradiation showed a green color solution, suggesting that the Ag-TBI-TPE cage could promote ROS production. The characteristic absorbance at 405 nm of the oxidized ABTS showed the same result, indicating that the Ag-TBI-TPE cage surely exhibited ICT and AIE characteristics that could promote ROS production after light irradiation.

To further confirm this result, electron paramagnetic resonance (EPR) was measured in the presence and absence of light irradiation in Ag$^+$, TBI-TPE, and the Ag-TBI-TPE cage solution. The result showed that only the Ag-TBI-TPE cage with UV light illumination had a strong signal using DMPO as the radical scavenger and turned out that it was the hydroxy radical (Fig. 2).

In other words, the Ag-TBI-TPE cage could catalyze ABTS (colourless) to oxide ABTS (green colour) under light irradiation due to the hydroxy radical production, verifying its promotion property for ROS species.

## Antibacterial activity of the Ag-TBI-TPE cage

Interactions between the Ag-TBI-TPE cage and two clinically significant pathogens were observed: the Gram-positive bacteria *Staphylococcus aureus* (*S. aureus*) and the Gram-negative bacteria *Escherichia coli* (*E. coli*) were observed. To investigate the interaction between the Ag-TBI-TPE cage with bacteria, the surface charge of *E. coli*, *S. aureus*, and the Ag-TBI-TPE cage were measured. The results showed that the zeta potentials of *E. coli*, *S. aureus,* and Ag-TBI-TPE cages were −22.66 mV, −21.23 mV, and 43.24 mV, respectively (Fig. 3A). Based on the above results, Ag-TBI-TPE cages could contact bacteria through the electrostatic interaction with the cell membrane. To further prove this result, the zeta potentials of Ag-TBI-TPE cages at different pH values were measured. As shown in Fig. S3,† at pH 7.0, the Ag-TBI-TPE cage was positively charged with the highest value among the cages for pH 3.0–10.0, providing better interaction with bacteria, which is in accordance with previous results.
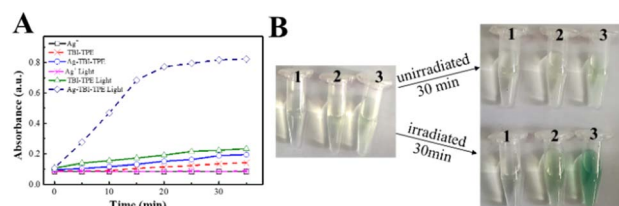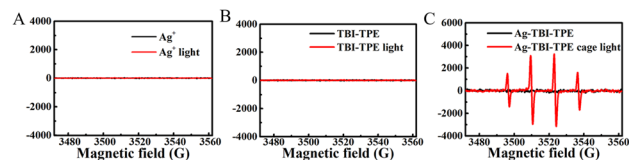


**Fig. 2** EPR spectra of the DMPO-OH adduct in the absence and presence of light irradiation (A) Ag$^+$, (B) TBI-TPE, (C) Ag-TBI-TPE cage.

Considering that the electrostatic interaction between the Ag-TBI-TPE cage and bacteria will result in membrane destruction, the agar diffusion test was performed to confirm the antibacterial activity of the Ag-TBI-TPE cage. As shown in Fig. 3B and C, TBI-TPE showed an antibacterial effect in both *E. coli* and *S. aureus*, the antibacterial circle diameters of Ag$^+$ and Ag-TBI-TPE cages for *E. coli* were 11.25 mm, 12.17 mm, for *S. aureus* are 11.50 mm, 14.50 mm, respectively. Furthermore, Ag nanoparticles were also used as a control to compare the antibacterial activity and the results showed that the antibacterial circle diameters of the Ag nanoparticles for *E. coli* was 11.10 mm and for *S. aureus* was 11.47 mm (Fig. S4†). Therefore, Ag$^+$, Ag nanoparticles, and Ag-TBI-TPE cages exhibited a good antibacterial activity, rather Ag-TBI-TPE cages had the best performance. In addition, the antimicrobial duration is an important factor to evaluate antibacterial materials. As a result, from the time-dependent experiment, the antibacterial circle diameter of the Ag-TBI-TPE cage against *E. coli* and *S. aureus* increased within 8 h, then slowly decreased, but still could maintain a high antibacterial efficiency for 82 h. However, the antibacterial activity lasting time of Ag$^+$ gradually decreased from 4 h but showed no obvious antibacterial activity after 32 h for *E. coli* and 48 h for *S. aureus* (Fig. S5†). In the solution, the Ag$^+$ release rate of the Ag-TBI-TPE cage was slower than that for AgNO$_3$ with the same concentration, due to the coordinating interaction between Ag$^+$ and TBI-TPE, which will give rise to a longer antibacterial lasting time.[44–48] These results further proved that the



**Fig. 1** (A) Time-dependent typical absorption curves of ABTS reaction solutions oxidized by TBI-TPE, Ag$^+$, and Ag-TBI-TPE cages at 405 nm. (B) The pictures of ABTS reaction solutions catalytically oxidized by (1) TBI-TPE, (2) Ag$^+$, and (3) Ag-TBI-TPE cage with and without light irradiation.
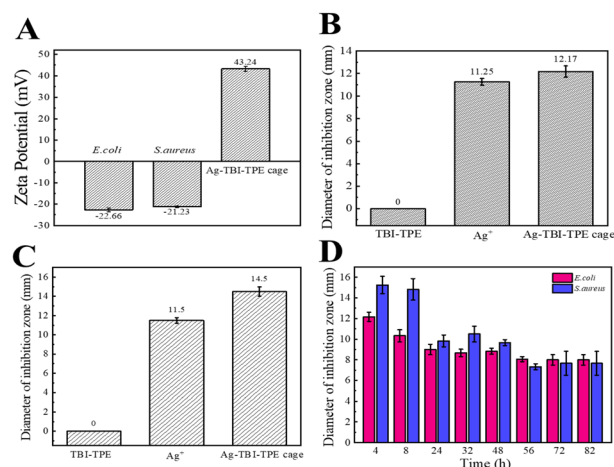
**Fig. 3** (A) Zeta potential of *E. coli*, *S. aureus*, and the Ag-TBI-TPE cage. Diameters of inhibition zones for (B) *E. coli*, (C) *S. aureus*. (D) Antibacterial effect of the Ag-TBI-TPE cage on *E. coli* and *S. aureus* by calculating the diameter of the inhibition zone over time.

Ag-TBI-TPE cage had excellent antibacterial activity with a longer lasting time compared to $Ag^+$.

Concentration-dependent bacterial growth inhibition by $Ag^+$ and Ag-TBI-TPE cages with and without light was investigated in detail. When the concentration ranged from 1 μM to 10 μM, the inhibition effect of $Ag^+$ and the Ag-TBI-TPE cage on *E. coli* and *S. aureus* was almost 100% after 30 min. However, at a low concentration of 0.5 μM, the inhibition of $Ag^+$ and Ag-TBI-TPE cage against *E. coli* and *S. aureus* were 64.33 ± 2.69%, 77.83 ± 3.63%, and 73.50 ± 1.16%, 80.83 ± 4.28% without light irradiation, respectively, indicating that the Ag-TBI-TPE cage exhibited stronger antibacterial activity than $Ag^+$ and showed a better effect on *S. aureus* than *E. coli* (Fig. S6A and B†). Moreover, time-dependent inhibition rates were also determined. As shown in Fig. S6C and D,† without light irradiation, the antibacterial inhibition rates of $Ag^+$ and the Ag-TBI-TPE cage on *E. coli* and *S. aureus* increased with time, and the Ag-TBI-TPE cage displayed a better inhibition effect.

ROS species could generate oxidative stresses in cells, which was able to damage the proteins and lipids and force cells to die *via* self-decomposition.[36,37,49–52] Therefore, due to the great ROS promotion property of the Ag-TBI-TPE cage, the antibacterial activity of the Ag-TBI-TPE cage under light irradiation conditions was tested. Firstly, the light irradiation effect on bacteria (without the Ag-TBI-TPE cage) was verified. As shown in Fig. S7,† after light irradiation (370 nm), the absorbance value of bacteria at 600 nm showed almost no change, indicating that light irradiation did not affect the normal growth of bacteria. It is worth noting that the most commonly used sterilization wavelength of UV irradiation is 240 nm to 280 nm, which is far from the one (370 nm) used in our experiments. This result was further supported by SEM measurements, before and after irradiating by the UV light (370 nm); the surfaces of *E. coli* and *S. aureus* were both smooth with complete rod-shaped and spherical morphologies, respectively, the same with native bacteria (Fig. S8†). The antibacterial activity of the Ag-TBI-TPE cage under UV light irradiation was revealed, and the results indicated that UV light irradiation could accelerate the antibacterial efficiency of the Ag-TBI-TPE cage (Fig. S6†). In addition, the DCFH-DA assay was employed to explore the promotion factor. As shown in Fig. S9,† compared with the Ag-TBI-TPE cage without light irradiation, there were many more ROS signals, which were detrimental to bacteria when the Ag-TBI-TPE cage was under UV light irradiation. These results revealed that light irradiation could promote the antibacterial properties of the Ag-TBI-TPE cage due to the production of toxic ROS. Based on the above results, owing to the positive charge of the Ag-TBI-TPE cage with a synergetic effect of photosensitivity, the antibacterial efficiency of the Ag-TBI-TPE cage could be further accelerated by light irradiation by promoting the production of toxic ROS.

## Mechanism of antibacterial behaviour

To reveal the antibacterial mechanism of the Ag-TBI-TPE cage, SEM images were taken to study the bacterial morphology. It is obvious that after 15 minutes of interaction with $Ag^+$ and $Ag^-$.
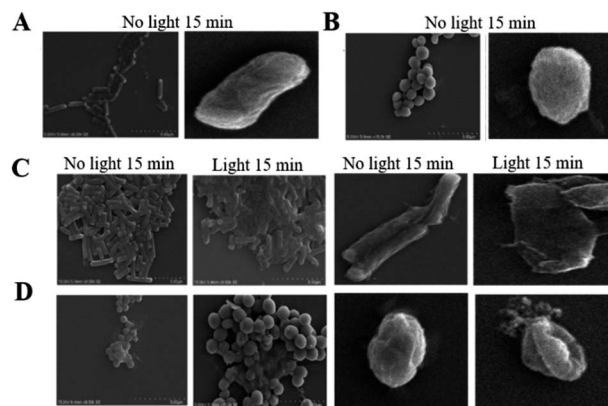


**Fig. 4** SEM images of $Ag^+$ interacting with (A) *E. coli*, (B) *S. aureus*, and Ag-TBI-TPE cage interacting with (C) *E. coli*, (D) *S. aureus*.

In the TBI-TPE cage without light irradiation, *E. coli*, and *S. aureus* showed rough surfaces and wrinkled cell walls, indicating damage to the cell membrane (Fig. 4). Besides, the Ag-TBI-TPE cage had a greater destructive effect on both *E. coli* and *S. aureus*. Moreover, with light irradiation, this damaging effect of the Ag-TBI-TPE cages could be accelerated. Causing further collapse of the bacterial structure. These results suggested that the antimicrobial mechanism of $Ag^+$ and Ag-TBI-TPE cage could be ascribed to membrane disruption. This result could be further supported by measuring the UV-Vis value at 260 nm, which was the characteristic absorbance of DNA/RNA that would leak out due to the disruption of the membrane. In Fig. S10,† after microorganisms contacted $Ag^+$ and the Ag-TBI-TPE cage, the adsorption intensities obviously increased, suggesting that DNA/RNA had leaked out of the cytomembranes, which confirmed the breaking of the cell membrane. In brief, considering that the Ag-TBI-TPE cage exhibited a ROS promotion effect, it could be concluded that the antibacterial mechanism of the Ag-TBI-TPE cage could be divided into two aspects. Firstly, the positively charged Ag-TBI-TPE cage can break the charge balance of the membrane, which plays an important role in antibacterial activity. Moreover, the production of excessively toxic ROS after light irradiation is also detrimental to bacteria, which could accelerate the destruction of the cell membrane.

## Biocompatibility and bio-safety of the Ag-TBI-TPE cage

Before applying the Ag-TBI-TPE cage-based antibacterial materials in practical applications, the biocompatibility and biosafety of the Ag-TBI-TPE cage are two important factors to be confirmed. The thermal and chemical stabilities of the Ag-TBI-TPE cage were confirmed in our previous report.[38] Moreover, the acute toxicity experiment was performed to evaluate the biocompatibility of the Ag-TBI-TPE cage. As shown in Fig. S11,† the experimental group exhibited the same phenomenon as the sterile physiological saline group, wherein obvious abnormal behavior and weight loss were not observed, indicating that the Ag-TBI-TPE cage was biocompatible and nontoxic.

In addition, the biosafety of the Ag-TBI-TPE cage was assessed by the cytotoxicity test and the hemolysis test on human

erythrocytes. The viability of the cell line was assessed *via* the MTT-based cell viability assay when the cell was co-cultured with the Ag-TBI-TPE cage. As a result, the Ag-TBI-TPE cage exhibited good biocompatibility, more than 94% of the cells were viable after treatment with the Ag-TBI-TPE cage, which was the same concentration in the antibacterial experiment (Fig. S12†). When using water as the positive control, the erythrocytes were broken and the supernatant turned red, which suggested that hemolysis occurred; however, physiological saline and the Ag-TBI-TPE cage group showed no hemolysis phenomenon. Besides, the sample group was shaken, and the erythrocytes were well-dispersed in solution, after a while, the cells sank at the bottom, which meant that the Ag-TBI-TPE cage did not agglutinate the human erythrocytes. Finally, when the concentration of the Ag-TBI-TPE cage was 10 μM, the hemolysis rate was $5.46 \pm 0.28\%$ which was acceptable in standard value, indicating the great biosafety of the Ag-TBI-TPE cage (Fig. S13†). Meanwhile, the histological analysis of the major organs from SD rats including heart, liver, kidney, lung, and spleen, showed that there were not any adverse effects and damages after the treatment with the Ag-TBI-TPE cage (Fig. S14†). The above results demonstrate that the Ag-TBI-TPE cage had excellent biocompatibility and showed no toxicity towards animals, which is beneficial for application in biological and medical fields.

## Wound healing *in vivo*

To investigate the antimicrobial activity and the wound healing ability of the Ag-TBI-TPE cage *in vivo*, the dorsal wound infection model of rats was studied for evaluating it *in vivo*. The traumas were photographed on day 1, day 3, and day 7 after the operation to expressly research the wound healing activity of the Ag-TBI-TPE cage (Fig. 5A and B). All the treated wound areas decreased over time. In detail, on day 7, the wound healing ratio of *S. aureus* (right) and *E. coli* (left) infected traumas in groups I, II, III, and IV were 73.56%, 59.71%; 67.74%, 51.38%; 90.84%, 83.48%; and 93.05%, 89.59%, respectively. The wound healing ratio of group III and group IV showed favorable accelerating wound healing ability, especially for group IV. Simultaneously, the wound healing rate of *S. aureus* infection in group III was slightly higher than that in *E. coli* infection. Through irradiation, the Ag-TBI-TPE cage could better promote wound healing. These observed results demonstrated that the Ag-TBI-TPE cage had an excellent wound-healing ability, especially upon irradiation with UV light.

The results of wound infection culture, which were sampled from wounds indicated that the bacteria in the wounds of group III and group IV were mainly eliminated (Fig. 5C). The effect of group IV was better than that of group III, and the effect on *S. aureus* was better than that on *E. coli*. This result also proved that irradiation using UV light could promote the antibacterial property of the Ag-TBI-TPE cage. The results of hematoxylin and eosin (H&E) staining further manifested that wounds were almost fully healed for the rats of group IV with treatment and irradiation on day 7 (Fig. 5D).

The wounds of groups I and II showed epidermal hyperplasia and inflammatory infiltration on day 3, while the wounds of
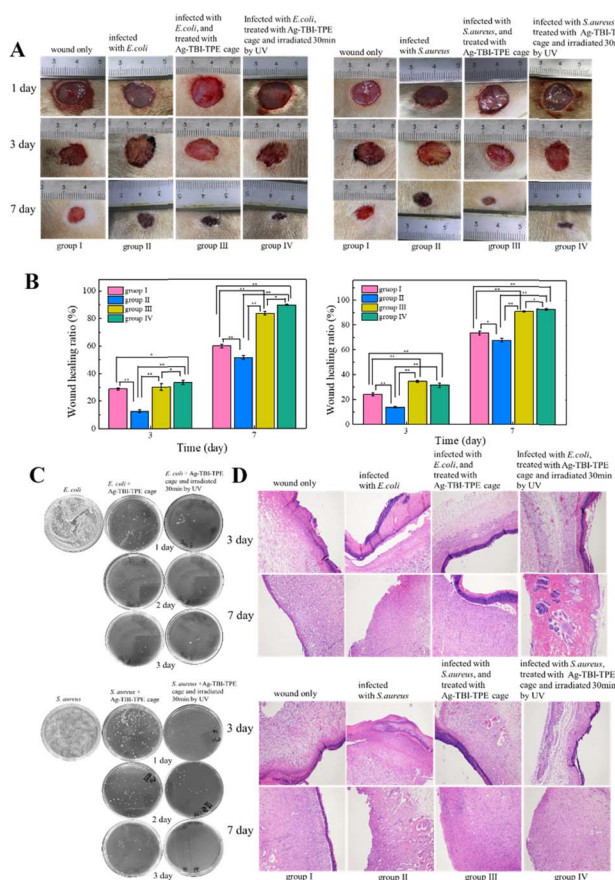


Fig. 5 The *in vivo* assessments of the Ag-TBI-TPE cage for wound healing. (A) Digital images of wound healing on day 1, day 3, and day 7, *in vivo*. (B) The wound healing ratio on day 3 and day 7 without and with treatment. $n = 5$, $*P < 0.05$, $**P < 0.01$, $***P < 0.001$. (C) Digital images of bacterial cultures on agar plate detached from the wounds. (D) Histological images of tissues stained with H&E after treatment on day 3 and day 7 (scale bar: 10 μm, magnification: 100×).

groups III and IV had entered the stage of repair. On day 7, the wounds of groups I and II had just entered the stage of repair, while the wounds of groups III and IV had entered the later stage of repair, and the necrotic tissue had gradually fallen off and tended to heal. The healing process of group IV was faster than that of group III, while the wound healing rate of infection with *S. aureus* was higher than that of the infection with *E. coli*. Based on these results, the Ag-TBI-TPE cage could eliminate bacteria effectively, and promote wound regeneration and healing, especially when irradiated by UV at the same time.

## Conclusion

In summary, a metal–organic cage named the Ag-TBI-TPE cage was synthesized using a facile process, which displayed significant antibacterial activity in both Gram-positive and Gram-negative bacteria. At the same time, the antibacterial effect of the Ag-TBI-TPE cage could be improved under UV irradiation, owing to its photosensitive nature to produce toxic ROS species. Besides, the biosafety and biocompatibility of the Ag-TBI-TPE cage were confirmed, and results suggested that the Ag-TBI-

TPE cage was non-toxic to animals. Based on these results, the Ag-TBI-TPE cage was applied to accelerate the healing process of the infected wounds *in vivo* with a satisfying effect. These important insights gained in our work will shed light on the design principles of efficient biomaterials for wound healing and will provide some new insights into different supramolecular metal coordination cages with unique properties for various applications.

## Ethical statement

All animal procedures for "A silver metal–organic cage with antibacterial activity for wound healing" (Animal Ethics Review No. 2021008) were performed in accordance with the Guidelines for Care and Use of Laboratory Animals of Quanzhou Medical College and approved by the Animal Ethics Committee of the Quanzhou Medical College.

## Conflicts of interest

There are no conflicts to declare.

## Acknowledgements

## Notes and references

1 L. Ying, Y. Tian, W. S. Zheng, Y. Feng, R. Huang, J. X. Shao, R. B. Tang, P. Wang, Y. X. Jia, J. J. Zhang, W. F. Zheng, G. Yang and X. Y. Jiang, *Small*, 2017, **13**, 1700130.

2 I. Jorgensen, M. Rayamajhi and E. A. Miao, *Nat. Rev. Immunol.*, 2017, **17**, 151–164.

3 V. Nizet, T. Ohtake, X. Lauth, J. Trowbridge, J. Rudisill, R. A. Dorschner, V. Pestonjamasp, J. Piraino, K. Huttner and R. L. Gallo, *Nature*, 2001, **414**, 454–457.

4 R. J. Wyke, *Gut*, 1987, **28**, 623–641.

5 N. D. Wolfe, C. P. Dunavan and J. Diamond, *Nature*, 2007, **447**, 279–283.

6 M. M. Levine and R. Edelman, *Epidemiol. Rev.*, 1984, **6**, 31–51.

7 M. C. Enright, D. A. Robinson, G. Randle, E. J. Feil, H. Grundmann and B. G. Spratt, *Proc. Natl. Acad. Sci. U. S. A.*, 2002, **99**, 7687.

8 M. C. Fisher, D. A. Henk, C. J. Briggs, J. S. Brownstein, L. C. Madoff, S. L. Mccraw and S. J. Gurr, *Nature*, 2012, **484**, 186–194.

9 A. Perdikaki, A. Galeou, G. Pilatos, I. Karatasios, N. K. Kanellopoulos, A. Prombona and G. N. Karanikolos, *ACS Appl. Mater. Interfaces*, 2016, **8**, 27498–27510.

10 X. Huang, N. Hu, X. Wang, Y. S. Zhang and R. Sun, *ACS Sustain. Chem. Eng.*, 2017, **5**, 2648–2655.

11 I. Irwansyah, Y. Q. Li, W. X. Shi, D. P. Qi, W. R. Leow, M. B. Y. Tang, S. Z. Li and X. D. Chen, *Adv. Mater.*, 2015, **27**, 648–654.

12 Y. Qin, L. L. Chen, W. Pu, P. Liu, S. X. Liu, Y. Li, X. L. Liu, Z. X. Lu, L. Y. Zheng and Q. E. Cao, *Chem. Commun.*, 2019, **55**, 2206–2209.

13 Q. L. Feng, J. Wu, G. Q. Chen, F. Z. Cui and J. O. Kim, *J. Biomed. Mater. Res.*, 2000, **52**, 662–668.

14 X. T. Ye, T. Feng, L. Li, T. J. Wang, P. Li and W. Huang, *Acta Biomater.*, 2021, **125**, 29–40.

15 B. H. Hu, C. Owh, P. L. Chee, W. R. Leow, X. Liu, Y. L. Wu, P. Guo, X. J. Loh and X. D. Chen, *Chem. Soc. Rev.*, 2018, **47**, 6917–6929.

16 C. C. Zhou, F. Y. Wang, H. Chen, M. Li, F. L. Qiao, Z. Liu, Y. B. Hou, C. X. Wu, Y. X. Fan, L. B. Liu, S. Wang and Y. L. Wang, *ACS Appl. Mater. Interface*, 2016, **8**, 4242–4249.

17 L. Fang, R. Ma, X. J. Gao, L. Chen, Y. Liu, Y. Huo, T. Wei, X. Wang, Q. Wang, H. Wang, C. Cui, Q. Shi, J. Jiang and L. Gao, *Adv. Sci.*, 2022, **9**, 2104341.

18 C. A. Strassert, M. Otter and R. Q. Albuquerque, *Angew. Chem., Int. Ed.*, 2009, **48**, 7928–7931.

19 W. B. Wu, D. Mao, F. Hu, S. D. Xu, C. Chen, C. J. Zhang, X. M. Cheng, Y. Y. Yuan, D. Ding, D. L. Kong and B. Liu, *Adv. Mater.*, 2017, **29**, 1700548.

20 X. Wu, M. Yang, J. S. Kim, R. Wang, G. Kim, J. Ha, H. Kim, Y. Cho, K. T. Nam and J. Yoon, *Angew. Chem., Int. Ed.*, 2022, **61**, 202200808.

21 G. Feng, C. J. Zhang, X. Lu and B. Liu, *ACS Omega*, 2017, **2**, 546–553.

22 X. J. Shi, S. H. P. Sung, J. H. C. Chau, Y. Li, Z. Liu, R. T. K. Kowk, J. Liu, P. Xiao, J. Zhang, B. Liu, J. W. Y. Lam and B. Z. Tang, *Small Methods*, 2020, **4**, 2000046.

23 H. Gao, D. Jiao, H. Ou, J. Zhang and D. Ding, *Acta Chim. Sin.*, 2021, **79**, 319–325.

24 Y. Li, Z. Zhao, J. Zhang, R. T. K. Kwok, S. Xie, R. Tang, Y. Jia, J. Yang, L. Wang, J. W. Y. Lam, W. Zheng, X. Jiang and B. Z. Tang, *Adv. Funct. Mater.*, 2018, **28**, 1804632.

25 T. Zhou, R. Hu, L. Wang, Y. Qiu, G. Zhang, Q. Deng, H. Zhang, P. Yin, B. Situ, C. Zhan, A. Qin and B. Z. Tang, *Angew. Chem., Int. Ed.*, 2020, **59**, 9952–9956.

26 B. Wang, S. Liu, X. Liu, R. Hu, A. Qin and B. Z. Tang, *Adv. Healthcare Mater.*, 2021, **10**, 2101067.

27 M. Kang, Z. Zhang, N. Song, M. Li, P. Sun, X. Chen, D. Wang and B. Z. Tang, *Aggregate*, 2020, **1**, 80–106.

28 Y. L. Balachandran and X. Jiang, *CCS Chem.*, 2022, **4**, 420–436.

29 X. Yang, Z. Ullah, J. F. Stoddart and C. T. Yavuz, *Chem. Rev.*, 2023, **123**, 4602–4634.

30 L. Zhu, X. Yang and J. K. Sun, *Chem. Commun.*, 2023, **59**, 6020–6023.

31 X. Yang, J. K. Sun, M. Kitta, H. Pang and Q. Xu, *Nat. Catal.*, 2018, **1**, 214–220.

32 M. L. Saha, X. Yan and P. J. Stang, *Acc. Chem. Res.*, 2016, **49**, 2527–2539.

33 X. Yang and Q. Xu, *Chem*, 2018, **4**, 403–404.

34 L. Zhu, S. Zhang, X. C. Yang, Q. Zhuang and J. K. Sun, *Small Methods*, 2022, **6**, 2200591.

35 L. Xu, Y. X. Wang, L. J. Chen and H. B. Yang, *Chem. Soc. Rev.*, 2015, **44**, 2148–2167.

36 C. Wang, J. Wang, K. Xue, M. Xiao, Z. Sun and C. Zhu, *Chem. Commun.*, 2022, **58**, 7058–7061.

37 X. Chen, H. Gao, Y. Deng, Q. Jin, J. Ji and D. Ding, *ACS Nano*, 2020, **14**, 5121–5134.

38 Z. Lu, Y. Cheng, W. Fan, S. Yang, X. Liu, Y. Qin, R. Zhao, L. Zheng and H. Zhang, *Chem. Commun.*, 2019, **55**, 8474–8477.

39 Z. Lu, Y. Liu, S. Lu, Y. Li, X. Liu, Y. Qin and L. Zheng, *RSC Adv.*, 2018, **8**, 19701–19706.

40 H. Ericsson, G. Tunevall and K. Wickman, *Scand. J. Clin. Lab. Invest.*, 1960, **12**, 414–422.

41 N. Nishiyama, F. Yuhei, K. Adachi, K. Inumaru and S. Yamazaki, *Appl. Catal., B*, 2015, **176**, 347–353.

42 J. Xiao, S. Chen, J. Yi, H. Zhang and G. A. Ameer, *Adv. Funct. Mater.*, 2017, **27**, 1604872.

43 R. Wang, J. Li, W. Chen, T. Xu, S. Yun, Z. Xu, Z. Xu, T. Sato, B. Chi and H. Xu, *Adv. Funct. Mater.*, 2017, **27**, 1604894.

44 Y. Li and J. Liu, *Mater. Horiz.*, 2021, **8**, 336–350.

45 K. Zheng, M. I. Setyawati, D. T. Leong and J. Xie, *Coord. Chem. Rev.*, 2018, **357**, 1–17.

46 B. Zakaria, C. Aouatef, D. Pierrick, D. Abdelatif, M. Filippo, G. Benoit and D. Slimane, *Inorg. Chim. Acta*, 2018, **482**, 34–47.

47 X. Lu, J. Ye, Y. Sun, R. F. Bogale, L. Zhao, P. Tian and G. Ning, *Dalton Trans.*, 2014, **43**, 10104–10113.

48 A. Liu, C. Wang, C. Wang, H. Fu, W. Peng, Y. Cao, H. Chu and A. Du, *J. Colloid Interface Sci.*, 2018, **512**, 730–739.

49 T. V. Slenters, J. L. Sagué, P. S. Brunetto, S. Zuber, A. Fleury, L. Mirolo, A. Y. Robin, M. Meuwly, O. Gordon, R. Landmann, A. U. Daniels and K. M. Fromm, *Materials*, 2010, **3**, 3407–3429.

50 Z. Liu, H. Zou, Z. Zhao, P. Zhang, G. Shan, R. T. K. Kwok, J. W. Y. Lam, L. Zheng and B. Z. Tang, *ACS Nano*, 2019, **13**, 11283–11293.

51 S. Liu, G. Feng, B. Z. Tang and B. Liu, *Chem. Sci.*, 2021, **12**, 6488–6506.

52 M. A. Kohanski, D. J. Dwyer, B. Hayete, C. A. Lawrence and J. J. Collins, *Cell*, 2007, **130**, 797–810.